Chapter 1

Neutron reflectometry.

C. FERMON, F. OTT and A. MENELLE

1.1 Introduction

Neutron reflectometry is a relatively new technique [1, 2]. It has been extensively used for solving soft matter problems like polymer mixing [3, 4]or the structure of liquids at the surface [5, 6]. The asset of neutrons for polymer studies is their small absorption compared to X-rays and the large contrast between ^{1}H and ^{2}H which allows selective labelling by deuteration.

In the late 80's, a new field of application of neutron reflectometry has emerged. Following the discovery of giant magnetoresistance in antiferromagnetically coupled multilayered films [7] and new phenomena in ultra-thin films, there has been an interest in the precise measurement of the magnetic moment directions in each layer and at the interface between layers. Owing the large magnetic coupling between the neutron and the magnetic moment, neutron reflectometry is a powerful tool for obtaining information about these magnetic configurations.

In this chapter, we give an overview of the experimental and theoretical methods used for neutron reflectometry. We focus on specular reflectivity. The corresponding theory is mainly derived from the previous work developed for X-rays.

In a first part, we will review the neutron-matter interactions. We then describe the non magnetic diffusion. In this case it is possible to introduce an optical index and give a treatment which is similar to X-ray reflectometry.

In a third part, the neutron spin is introduced. In this case, optical indexes cannot be used any more and it is necessary to completely solve the Schrödinger equation.

We then describe the different aspects of data processing and the problems related to the surface roughness. Two types of neutron reflectometers are then described : fixed wavelength two axis reflectometers and time of flight spectrometers.

We then illustrate the use of neutron reflectivity in the field of polymers films and in the field of magnetic layers.

Notations

b, b_α	diffusion length of a nucleus, mean diffusion length of a layer α
b_0	part of the diffusion length independent of the spin.
b_n	spin dependent part of the diffusion length.
b"	imaginary part of the diffusion length
E_0, E_α	energy of the neutron in the vacuum and in a layer.
e	charge of the electron
d, d_α	thickness of a layer.
g	Landé factor, (g =2)
$\hbar$	Planck constant
$\mathbf{I}$	nuclear spin operator
$\mathbf{k}$	wave vector
$\mathbf{M}, \mathbf{M}_\alpha$	magnetic moment of an electron and of a layer
m	neutron mass
m_e	electron mass
n_α	refraction index of the layer α
p	p = 2.696 fm, conversion factor of magnetization to effective diffusion length.
$\mathbf{q}$	diffusion vector
$\mathbf{s}$	spin operator of the electron
σ	Pauli operator associated to the neutron spin.
V_α	volume of the layer α
V(r)	interaction hamiltonian
g_n	$g_n = 1.9132$, nuclear Landé factor of the neutron
λ, λ_0	neutron wavelength
μ_B	Bohr magneton
μ_n	nuclear magneton
ρ_α	atomic density of the layer α (atoms per cm^3)
σ_α	absorption
$\theta_\alpha, \varphi_\alpha$	spherical angles of the magnetization of the layer α
θ_{inc}, θ_{ref}	incident and reflected angles of the neutron beam

$\mathbf{M_s} = -\mathbf{g}\ \mu_\mathbf{B}\ \sigma$,

$\mu_B = \frac{e\hbar}{2m_e} = 9,27.10^{-24}\ J.T^{-1}$, $\mu_n = \frac{e\hbar}{2m_p} = 5.05.10^{-27}\ J.T^{-1}$

$\theta(x)$ is the Heavyside function defined by :

$$\begin{cases} \theta(x) = 1 \quad \text{when} \quad x > 0 \\ \theta(x) = 1/2 \quad \text{when} \quad x = 0 \\ \theta(x) = 0 \quad \text{when} \quad x < 0 \end{cases}$$

We call "up" (resp. "down") the neutron polarization parallel (resp. anti-parallel) to the external applied magnetic field.

"Down-up" designates a polarized down incident beam and polarized up detected beam.

"Down-up" and "up-down" are called spin-flip processes.

1.2 Schrödinger equation and neutron-matter interactions.

1.2.1 Schrödinger equation

The neutron can be described by a wave of wavelength λ, of wave vector :

$$k_0 = \frac{2\pi}{\lambda} \tag{1.1}$$

and of energy

$$\mathcal{E}_0 = \frac{\hbar^2 k_0^2}{2m} \tag{1.2}$$

Its wave function verifies the Schrödinger equation :

$$\frac{\hbar^2}{2m}\frac{d^2\psi}{dr^2} + [\mathcal{E} - V(r)]\,\psi = 0 \tag{1.3}$$

where m is the neutron mass, $\mathcal{E}$ its energy and V the interaction potential.

The neutron is a spin 1/2 particle so that $\psi(r)$ can be expressed on the base of the two spin states :

$$\psi_+(r)\,|+\rangle + \psi_-(r)\,|-\rangle\,. \tag{1.4}$$

When there is an external or internal magnetic field, an "up" (resp. "down") neutron designates a neutron in the eigenstate $|+\rangle$ (resp. |-$\rangle$).

In the following the space dependence index ($\mathbf{r}$) will often be dropped.

1.2.2 Neutron-matter interaction.

The two main interactions are the strong interaction with the nuclei and the magnetic interaction with the existing magnetic moments (nuclear and electronic). There are a large number of second order interactions which are described in [8].

Neutron nucleus interaction : Fermi pseudo potential

The diffusion of a neutron on a nucleus comes mainly from the strong interaction. The interaction potential is large but its extension is much smaller than the wavelength of the neutron. Hence this interaction can be considered as ponctual and isotropic. within the Born approximation, it can be modelled by a potential of the form [9] :

$$V_F(r) = b\left(\frac{2\pi\hbar^2}{m}\right)\delta(r) \tag{1.5}$$

where b is the scattering length. Its value depends on the nucleus and the nuclear spin of the nucleus. Formally it is written :

$$b = b_0 + \frac{1}{2}b_n\mathbf{I}.\sigma \tag{1.6}$$

We often call b^+ and b^- the values measured for the two states $|+\rangle$ and |-$\rangle$ of the neutron spin.

It can be shown that [10] :

$$\left\{\begin{array}{l} b^+ = b_0 + \frac{1}{2}b_n I \\ b^- = b_0 - \frac{1}{2}b_n(I+1) \end{array}\right. \tag{1.7}$$

Absorption and incoherent diffusion.

A neutron can be absorbed or incoherently diffused. This introduces an imaginary part b'' in the scattering length b :

$$b^{"} = (k_0/4\pi)\,\sigma_a \tag{1.8}$$

The absorption is negligible for thin films except for some elements : Gd, Sm, B and Cd. These elements present some nuclear resonances which increase strongly the absorption.

Incoherent diffusion comes from the existence of different isotopes or different nuclear spin states in the layer. This appears as a q-independent background in the experiments and can be treated as an absorption plus a flat background. The incoherent diffusion is particularly important for hydrogenated layers but it is small for deuterated layers.

Magnetic interaction

The main magnetic interaction is the dipolar interaction of the neutron spin with the magnetic field created by the unpaired electrons of the magnetic atoms. This field contains 2 terms, the orbital part and the spin part :

$$\mathbf{B} = \frac{\mu_0}{4\pi}\left(\nabla\times\left\{\frac{\mu_\mathbf{e}\times\mathbf{R}}{|\mathbf{R}|^3}\right\} - \frac{e\,\mathbf{v_e}\times\mathbf{R}}{|\mathbf{R}|^3}\right) \tag{1.9}$$

where $\mu_e = -2\mu_B\sigma$ is the magnetic moment of the electron, μ_B is the Bohr magneton, $\mathbf{v}_e$ is the speed of the electron.

The magnetic interaction is :

$$V_M(r) = -g_n\mu_n\sigma.\mathbf{B} \tag{1.10}$$

Neutron reflectivity does not allow to separate the orbital and spin contributions, it is only sensitive to the internal magnetic field.

The Zeeman interaction

It is the interaction between the neutron spin with the external magnetic field $\mathbf{B}_0$:

$$V_Z(r) = -g_n\mu_n\sigma.\mathbf{B}_0 \tag{1.11}$$

1.2.3 Propagation of a neutron in an homogeneous magnetic field.

There are two ways of describing a neutron propagating in an homogeneous magnetic field B_0. The first one is given by solving the time dependent Schrödinger equation. One separates the spatial and spin coordinates and considers that the neutron propagates at a constant speed and that the field induces a spin precession. The wave function is then time dependent :

$$\psi = e^{i(k_x x + k_y y + k_z z)}\left(\alpha e^{i\omega_L t}\left|+\right\rangle + \beta e^{-i\omega_L t}\left|-\right\rangle\right) \tag{1.12}$$

where $\omega_L = -\gamma B_0$ is the Larmor frequency of the neutron spin and $\alpha^2 + \beta^2 = 1$.

The second description consists in solving the stationnary wave equation with a potential written as :

$$V_Z(r) = -g_n\mu_n\sigma.\mathbf{B_0} \tag{1.13}$$

If the quantization axis is taken along the magnetic field direction (Oz), the Schrödinger equation is written :

$$\frac{\hbar^2}{2m}\frac{d^2\psi}{dr^2} + \left[\mathcal{E} + g_n\mu_n\sigma_z.\mathbf{B}_0\right]\psi = 0 \tag{1.14}$$

Since the potential is only z dependent, the wave function is of the form :

$$\psi = e^{i(k_x x + k_y y)}\left(\psi_z^+\left|+\right\rangle + \psi_z^-\left|-\right\rangle\right) \tag{1.15}$$

We obtain an equation for each spinor component :

$$\frac{\hbar^2}{2m}\frac{d^2\psi_z^\pm}{dr^2} + \left(\mathcal{E} - \frac{\hbar^2(k_x^2 + k_y^2)}{2m} \pm g_n\mu_n B_0\right)\psi_z^\pm = 0 \tag{1.16}$$

Whose solutions are :

$$\psi_z^\pm = a^\pm e^{ik_0^\pm z} \tag{1.17}$$

with

$$k_0^\pm = \left[\frac{2m}{\hbar^2}\mathcal{E} - (k_x^2 + k_y^2) \pm \frac{2m}{\hbar^2}g_n\mu_n B_0\right]^{1/2} \tag{1.18}$$

The physical meaning of the two values k^+ and k^- is that a spin 'up' neutron goes faster than a spin 'down' neutron. This energy difference (or speed difference) can be measured in reflectometry for large magnetic fields.

In the case where the neutron is not in an eigenstate but quantified along the x axis for example, its state at $t = 0$ is $\frac{1}{\sqrt{2}}(\left|+\right\rangle + \left|-\right\rangle)$. We deduce from (1.18) that the neutron separates in two wave paquets, one slower than the other.

The two solutions (1.12) and (1.17) are not identical. The exact solution is given by (1.12). However, at the first order in $|V_Z|/\mathcal{E}$, the two equations are identical. In the following formalism we will use the form given by equation (1.17) because the time dependent wave function leads to much more complex mathematical manipulations.

In a 1 tesla field and for a neutron of wavelength of 0.4 nm, $|V_Z|/\mathcal{E} = 0.01$.

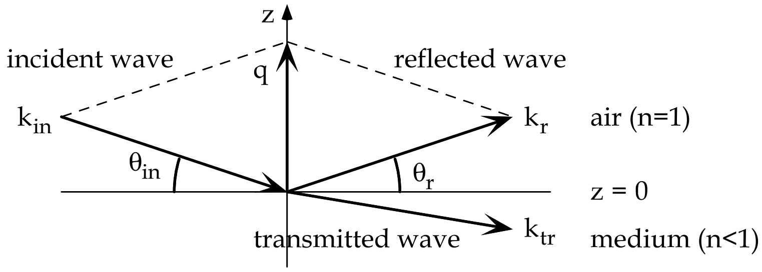

Figure 1.1: Reflectivity on a perfect surface.

1.3 Reflectivity on non magnetic systems.

For non magnetic systems we can introduce the notion of optical indexes. It is an approach similar to the X-ray formalism (chapter I and II). It can be applied to neutron reflectometry on soft matter [13] and non magnetic systems.

We consider a neutron beam, reflected by a perfect surface with an incident angle θ. As in chapter II, the surface is defined by the interface between the air ($n = 1$) and a material with an optical refractive index n that we will derive.

In the vacuum, the energy of the neutron is given by $\mathcal{E} = \frac{\hbar^2 k_{in}^2}{2m} = \frac{h^2}{2m\lambda^2}$

Let $\mathbf{q} = \mathbf{k_r} - \mathbf{k_{in}}$ be the scattering wave vector. The projection of the scattering wave vector on the z axis (perpendicular to the surface) is given by :

$$q_z = \frac{4\pi}{\lambda} \sin\theta_{inc} \tag{1.19}$$

1.3.1 Neutron optical indexes.

The neutron indexes are very different from X rays indexes and we will determine their expression from the Schrödinger equation.

We suppose that the interaction potential V in the medium is independent on the in-plane coordinates x and y.

In the absence of any magnetic field, the Schrödinger equation can be written :

$$\frac{\hbar^2}{2m}\frac{d^2\psi}{dr^2} + [\mathcal{E} - V]\,\psi = 0 \tag{1.20}$$

The equation (1.20) can be written in the form of a Helmholtz propagation equation similar to the electromagnetic case :

$$\frac{d^2\psi}{dr^2} + k^2\psi = 0 \tag{1.21}$$

with

$$k^2 = \frac{2m}{\hbar^2}[\mathcal{E} - V] \tag{1.22}$$

With define the optical index as :

$$n^2 = \frac{k^2}{k_0^2} \tag{1.23}$$

The mean potential V_z in the medium is given by the integration of the Fermi pseudo-potential.

$$V = \frac{1}{v}\int_v V(r)dr = \frac{2\pi\hbar^2}{m} b\rho \tag{1.24}$$

where ρ is the number of atoms per unit volume.

The expression of the optical index n can be written :

$$n^2 = 1 - \frac{V}{\mathcal{E}} = 1 - \frac{\lambda^2}{\pi}\rho b \tag{1.25}$$

The optical index is in most cases smaller than one except for the material with a negative scattering length (e.g. Ti and Mn). The quantity $1 - n$ is of order 10^{-5} thus the expression of n is given by :

$$n \approx 1 - \frac{\lambda^2}{2\pi}\rho b \tag{1.26}$$

1.3.2 Total reflection-Critical angle.

At the interface between two media, the Snell's law applies :

$$\cos\theta_{in} = n\cos\theta_{tr} \tag{1.27}$$

Since we have shown that the index is smaller than one, for angles $\theta \leq \theta_c$, there is a total reflection of the incident wave as in the case of X-ray reflection. The critical angle θ_c is given by the condition $\theta_{tr} = 0$, i.e. :

$$\cos\theta_c = n \tag{1.28}$$

Since θ_c is very small it is possible to use a Taylor expansion. Using (1.26) and (1.28) the expression of θ_c is given by :

$$\theta_c = \sqrt{\frac{\rho b}{\pi}}\lambda \tag{1.29}$$

The corresponding critical wave vector is :

$$q_c = \frac{4\pi sin\theta_c}{\lambda} = 4\sqrt{\pi\rho b} \tag{1.30}$$

1.3.3 Determination of scattering length and optical index

In the case of pure materials, the knowledge of b and ρ fully characterizes the material. In the case of solids of the type A_xB_y for example, one should consider unit cells. The volume of the unit cell allows to calculate a density ρ of unit cells per unit volume. The average b_{av} in the unit cell is simply given by $b_{av} = \frac{xb_A+yb_B}{x+y}$. The value ρb_{av} can be used to calculate the index of the material. The case of liquids and polymers is more complex since it is usually more difficult to define a "unit cell". Thus, the best method is to calibrate the index of each polymer or liquid that you want to study.

1.3.4 Reflection on a homogeneous medium

As has been shown by the equation (1.20) the problem of the reflection of a neutron beam on a non magnetic medium can be treated exactly in the same way as the reflection of X-rays. Since the potential V is only z dependent, the Schrödinger equation (1.20) reduces to the 1 dimensional equation :

$$\frac{\hbar^2}{2m}\frac{d^2\psi_z}{dz^2} + [\mathcal{E}_z - V_z]\,\psi_z = 0 \tag{1.31}$$

with a wave function of the form $\psi = e^{i(k_{inx}x+k_{iny}y)}\psi_z$.
In the medium, the general solution is given by :

$$\psi_z = Ae^{ik_{trz}z} + Be^{-ik_{trz}z} \tag{1.32}$$

The transmitted wave vector can be related to the incident wave vector using (1.22) :

$$k^2 = \frac{2m}{\hbar^2}\left[\mathcal{E} - V\right] = k_{in}^2 - 4\pi\rho b \tag{1.33}$$

At the interface we have to apply the continuity condition on ψ and $\nabla\psi$. In a way similar to the X-ray case, it is then possible to show that the parallel components of the incident wave are continuous [9].

The continuity of the parallel components allows us to write :

$$k_{tr,z}^2 = k_{in,z}^2 - 4\pi b\rho \tag{1.34}$$

Material	$b_n(fm)$	$\rho(10^{28}m^{-3})$	$\rho b(10^{13}m^{-2})$	$\delta(10^{-6})$	$q_c(nm^{-1})$	observation
H	-3.73					hydrogen
D (^{2}H)	6.67					deuterium
C	6.64	11.3	75	19.1	0.19	graphite
C	6.64	17.6	117	29.8	0.24	diamond
O	5.80					
Si	4.15	5.00	20.8	5.28	0.10	
Ti	-3.44	5.66	-19.5	-5.0	-	
Fe	9.45	8.50	80.3	20.45	0.20	
Co	2.49	8.97	32.6	8.29	0.13	
Ni	10.3	9.14	94.1	24.0	0.22	
Cu	7.72	8.45	65.2	16.6	0.18	
Ag	5.92	5.85	34.6	8.82	0.13	
Au	7.63	5.90	45	11.5	0.15	
H_2O	-1.68	3.35	-5.63	-1.43	-	
D_2O	19.1	3.34	63.8	16.2	0.18	
SiO_2	15.8	2.51	39.7	10.1	0.14	
GaAs	13.9	2.21	30.7	7.82	0.12	
Al_2O_3	24.3	2.34	56.9	14.5	0.17	sapphire
pyrex			42	10.7	0.14	
C_8H_8	23.2	0.61	14.2	3.6	0.084	polystyrene
C_8D_8	106.5	0.61	65	16.5	0.18	

Table 1.1: Scattering length, atomic density, optical index (at 0.4 nm), and critical wave-vector of some common materials. Exhaustive data can be found at *'www.neutron.anl.gov'*.

Considering the equations (1.21) and (1.34), the problems of neutron and X-ray reflectivity are formally the same. It is possible to use the same formalism as the one developed in chapter 3 for X-ray reflectivity.

In particular, it is possible to use the classical Fresnel formula. The reflected and transmitted intensities are given by :

$$R = \frac{\sin\theta_i - n\sin\theta_{tr}}{\sin\theta_i + n\sin\theta_{tr}} \tag{1.35}$$

$$T = \frac{2\sin\theta_i}{\sin\theta_i + n\sin\theta_{tr}} \tag{1.36}$$

In terms of scattering wave vector, the reflected intensity is given by :

$$R = \left|\frac{k_0 - k_{tr}}{k_0 + k_{tr}}\right|^2 \tag{1.37}$$

The figure 1.2 shows a typical curve calculated for a perfect surface.

1.4 Neutron reflectivity on magnetic systems

If the system is magnetic or if there is an external magnetic field on the sample, we need to take into account the spin of the neutron. It is not possible to use optical indexes and it is always necessary to completely solve the Schrödinger equation [14, 15, 16].

In the case of homogeneous, infinite magnetic layers, the problem can be solved using a formalism very similar to the non magnetic case developed in the previous part.

1.4.1 Interaction of the neutron with an infinite homogeneous layer

We consider a magnetic layer of thickness d, the neutron interacts with the different unpaired electrons. We perform a direct integration on the layer in order to obtain the potential V for the Schrödinger equation.

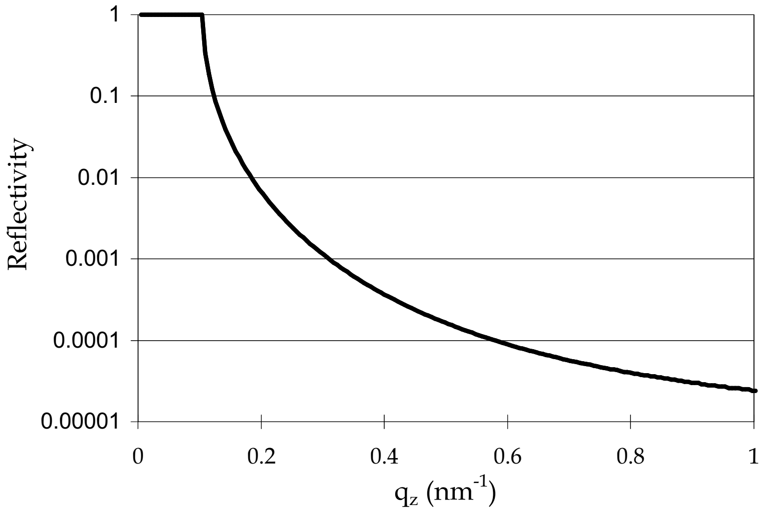

Figure 1.2: reflected intensity as a function of q_z for a silicon substrate.

The magnetic interaction

A first approach is to assume that the neutron is sensitive to the internal magnetic field in the magnetic layer. The interaction potential is then written :

$$-g_n\mu_n\sigma.\left[\mu_\mathbf{0}\left(\mathbf{1}-\mathbf{D}\right)\mathbf{M}+\mathbf{B_0}\right] \tag{1.38}$$

where $\mathbf{M}$ is the magnetization of the layer, D is the demagnetizing factor and $\mathbf{B_0}$ is the external magnetic field. In the case of an infinite magnetic thin film, $(1-D)\,\mathbf{M}$ is equal o the in-plane component of the magnetization $\mathbf{M}_{//}$.

It is possible to demonstrate this result but the calculations are somewhat lengthy. It is developed in the next page for the interested reader but it can be skipped at the first reading.

The magnetic interaction can be written :

$$-g_n\mu_n\sigma.\mathbf{B}=-\mathbf{g_n}\mu_\mathbf{n}\sigma.\left(\nabla\times\left\{\frac{\mu_\mathbf{e}\times\mathbf{R}}{|\mathbf{R}|^\mathbf{3}}\right\}-\frac{\mathbf{e}}{\mathbf{c}}\frac{\mathbf{v_e}\times\mathbf{R}}{|\mathbf{R}|^\mathbf{3}}\right) \tag{1.39}$$

or

$$-g_n\mu_n\left\{\sigma.\nabla\times\left(\frac{\mu_e\times\mathbf{R}}{|R|^3}\right)-\frac{e}{2m_ec}(\mathbf{p}_e.\frac{\sigma\times\mathbf{R}}{|\mathbf{R}|^3}+\frac{\sigma\times\mathbf{R}}{|\mathbf{R}|^3}.\mathbf{p}_e\right\} \tag{1.40}$$

with

$$\mathbf{p}_e=-i\hbar\nabla_e \tag{1.41}$$

If we first consider only the spin dependent part of the interaction, we can write :

$$\nabla\times(\frac{\mu_e\times\mathbf{r}}{r^3})=-\nabla\times(\mu_e\times\nabla(\frac{1}{\mathbf{r}}))=\frac{1}{2\pi^2}\int\frac{1}{q^2}(\mathbf{q}\times(\mu_e\times\mathbf{q}))\exp(i\mathbf{q}.\mathbf{r})d\mathbf{q} \tag{1.42}$$

Integration on a homogeneous layer

We suppose a constant atomic density ρ. We replace $\mathbf{r}$ by $\mathbf{r}+\mathbf{r_0}$. where $\mathbf{r_0}$ is the distance between the neutron and the centre of the layer. $\mathbf{r}$ is the distance the centre and the volume $d\mathbf{r}$ in the layer.

The spin dependent part of the interaction is :

$$2\gamma\mu_n\mu_B\sigma.\frac{\mathbf{1}}{\mathbf{2\pi^2}}\int\frac{\mathbf{1}}{\mathbf{q^2}}\int\limits_\mathbf{V}\rho(\mathbf{r})(\mathbf{q}\times\overline{\mathbf{s}}(\mathbf{r})\times\mathbf{q})\exp(\mathbf{iq.r_0})\exp(\mathbf{iq.r})\mathbf{drdq} \tag{1.43}$$

where $\rho(r)$ is the density and $\overline{s}(\mathbf{r})=\overline{\mathbf{s}}$ is the mean value of the spin magnetization in the volume dr.

The two first integrations over x and y give Dirac distributions.

$$4\mu_N\gamma\mu_B\rho\sigma.\int\frac{1}{q_z^2}\int_{-L/2}^{L/2}dr_z(\mathbf{q}_z\times\hat{s}\times\mathbf{q}_z)\exp(i\mathbf{q_z}.\mathbf{r_{0z}})\exp(i\mathbf{q_z}\mathbf{r_z})d\mathbf{q}_z \tag{1.44}$$

The third integration gives:

$$8\pi\mu_n\gamma\mu_B\rho\sigma.\overline{s}_{//}\left[\theta(r_{0z}+L/2)-\theta(r_{0z}-L/2)\right] \tag{1.45}$$

We can do the same calculation on the orbital part and we obtain :

$$\frac{2\pi\hbar^2}{m}p\sigma.\mathbf{M}_{//}\rho\left[\theta(r_{0z}+L/2)-\theta(r_{0z}-L/2)\right] \tag{1.46}$$

with $p = 2.696fm$.

$\mathbf{M}_{//}$ is given in μ_B per atom and represents the in-plane component of the magnetization and not necessarily the magnetization perpendicular to the wave vector.

Conclusion

From equation (1.46), we can deduce two very important points : it is only possible to measure the in-plane magnetization and the magnetic interaction is zero out of the layer.

These two properties are essential, the first is the main limitation of the use of neutrons for the study of magnetic thin films, the second is the justification of solving the Schrödinger equation in each layer, independently of the others. Thus the formalism developed for non magnetic systems can be adapted to the magnetic case with however some complications.

1.4.2 Solution of the Schrödinger Equation

The interaction potential for a layer α is given by :

$$V_\alpha = \frac{2\pi\hbar^2}{m}\rho_\alpha b_\alpha - \frac{2\pi\hbar^2}{m}\rho_\alpha p\sigma.\mathbf{M}_{\alpha//} - \mathbf{g_n}\mu_\mathbf{n}\sigma.\mathbf{B_0} \tag{1.47}$$

We introduce an effective field $\mathbf{B}_{eff}$ defined by :

$$\mathbf{B}_{eff} = \mathbf{B}_0 + \mu_0\mathbf{M}_{//} \tag{1.48}$$

If we introduce the spherical angles θ and ϕ to describe the effective field :

$$\left\{\begin{array}{l} B_{eff,\alpha x} = B_{0x} + \mu_0 M_{\alpha x} = B_{eff,\alpha}\sin(\theta_\alpha)\cos(\varphi_\alpha) \\ B_{eff,\alpha y} = B_{0y} + \mu_0 M_{\alpha y} = B_{eff,\alpha}\sin(\theta_\alpha)\sin(\varphi_\alpha) \\ B_{eff,\alpha z} = B_{0z} = B_{eff,\alpha}\cos(\theta_\alpha) \end{array}\right. \tag{1.49}$$

The interaction potential V can then written in the compact form :

$$V_\alpha = \frac{2\pi\hbar^2}{m}\rho_\alpha b_\alpha - g_n\mu_n\sigma.\mathbf{B}_{\mathbf{eff},\alpha} \tag{1.50}$$

The Schrödinger equation :

$$-\frac{\hbar^2}{2m}\Delta\psi + V(r)\psi = \mathcal{E}\psi \tag{1.51}$$

is a vectorial equation in the basis of the two spin states $|+\rangle$ and $|-\rangle$. We have to solve the Schrödinger equation (1.3) with a wave function expressed with its two spinors components ψ_+ and ψ_-.

It can be written explicitly as :

$$\begin{aligned} &- \frac{\hbar^2}{2m}\Delta\begin{pmatrix}\psi_+\\ \psi_-\end{pmatrix} + \left(\frac{2\pi\hbar^2}{m}\rho_\alpha b_\alpha\right)\begin{pmatrix}\psi_+\\ \psi_-\end{pmatrix} \\ &- g_n\mu_n\left(B_{eff,x}\sigma_x + B_{eff,y}\sigma_y + B_{eff,z}\sigma_z\right)\begin{pmatrix}\psi_+\\ \psi_-\end{pmatrix} = \mathcal{E}\begin{pmatrix}\psi_+\\ \psi_-\end{pmatrix} \end{aligned} \tag{1.52}$$

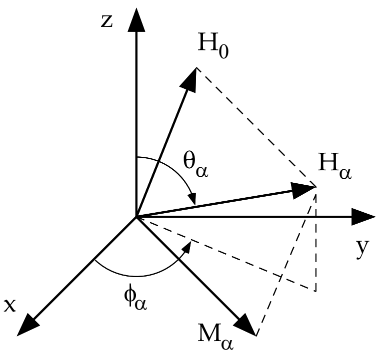

Figure 1.3: Effective field $\mathbf{B}_{\mathbf{eff},\alpha}$ in the layer, sum of the external field $\mathbf{B_0}$ and of the magnetization of the layer $\mathbf{M}_\alpha$. Definition of the spherical coordinates ϕ_α and θ_α.

where the Pauli spin operators σ are given by :

$$\sigma_x = \begin{pmatrix} 0 & 1 \\ 1 & 0 \end{pmatrix} \sigma_y = \begin{pmatrix} 0 & -i \\ i & 0 \end{pmatrix} \sigma_z = \begin{pmatrix} 1 & 0 \\ 0 & 1 \end{pmatrix}$$

We obtain the two coupled equations involving the two spinor components ψ_+ and ψ_- :

$$\begin{aligned} & \left(-\frac{\hbar^2}{2m}\nabla^2 + \frac{2\pi\hbar^2}{m} b_\alpha \rho_\alpha - g_n \mu_n B_{eff,z}\right) \psi_+(r) \\ + \quad & (-g_n \mu_n B_{eff,x} + i\gamma\mu_n B_{eff,y})\, \psi_-(r) = \mathcal{E}\psi_+(r) \\ & \left(-\frac{\hbar^2}{2m}\nabla^2 + \frac{2\pi\hbar^2}{m} b_\alpha \rho_\alpha + \gamma \mu_n B_{eff,z}\right) \psi_-(r) \\ + \quad & (-g_n \mu_n H_{eff,x} - i\gamma\mu_n H_{eff,y})\, \psi_+(r) = \mathcal{E}\psi_-(r) \end{aligned} \tag{1.53}$$

1.4.3 General Solution

We search solutions of the form : $\psi_+(\mathbf{r}) = \mathbf{a}_+ \exp(\mathbf{ikr})$ and $\psi_-(\mathbf{r}) = \mathbf{a}_- \exp(\mathbf{ikr})$

The values possible values for $\mathbf{k}$ are given by the possibility of finding non zero solutions of the previous system (i.e. zero determinant condition). This conditions gives four possible values for $\mathbf{k}$

$$k_\alpha^{\pm 2} = \frac{2m}{\hbar^2}\mathcal{E} - 4\pi\rho_\alpha b_\alpha \pm \frac{2m\gamma\mu_n}{\hbar^2} |B_\alpha| \tag{1.54}$$

where

A general solution with the form

$$\exp(ik_{//,\alpha}.r_{//}).\left(a\exp(ik^+_{z,\alpha}.z) + b\exp(-ik^+_{z,\alpha z}.z) + c\exp(ik^-_{z,\alpha z}.z) + d\exp(-ik^-_{z,\alpha z}.z)\right) \tag{1.55}$$

is not valid when there is an external magnetic field because $k^+_{//,0} \neq k^-_{//,0}$.

As this point there are two ways to solve the problem.

The first way is to solve the problem for each eigenstate $|+\rangle$ and $|$-$\rangle$.

The second way consists in taking the good general solution which is written :

$$\begin{aligned} & \exp(ik^{++}_{//,\alpha}.r_{//}).\left(a\exp(ik^{++}_{z,\alpha}.z) + b\exp(-ik^{++}_{z,\alpha}.z)\right) \\ + \quad & \exp(ik^{--}_{//,\alpha}.r_{//}).(c\exp(ik^{--}_{z,\alpha}.z) + d\exp(-ik^{--}_{z,\alpha}.z)) \\ + \quad & \exp(ik^{+-}_{//,\alpha}.r_{//}).\left(e\exp(ik^{+-}_{z,\alpha}.z) + f\exp(-ik^{+-}_{z,\alpha}.z)\right) \\ + \quad & \exp(ik^{-+}_{//,\alpha}.r_{//}).(g\exp(ik^{-+}_{z,\alpha}.z) + h\exp(-ik^{-+}_{z,\alpha}.z)) \end{aligned} \tag{1.56}$$

with

$$\left\{\begin{array}{ll} k_\alpha^{++2} = k_\alpha^{+2}, & k_{//,\alpha}^{++2} = k_{//,0}^{+2} \\ k_\alpha^{+-2} = k_\alpha^{+2}, & k_{//,\alpha}^{+-2} = k_{//,0}^{-2} \\ k_\alpha^{-+2} = k_\alpha^{-2}, & k_{//,\alpha}^{-+2} = k_{//,0}^{+2} \\ k_\alpha^{--2} = k_\alpha^{-2}, & k_{//,\alpha}^{--2} = k_{//,0}^{-2} \end{array}\right. \tag{1.57}$$

The solution of equation (1.4.2) is the solution (1.56) rotated by the angles of the quantization axis.

$$\begin{aligned} \psi_\alpha^+(r) &= \exp(ik_{//,\alpha}^{++} r_{//})(a_\alpha^{++}\exp(i\,k_{z,\alpha}^{++}z) + b_\alpha^{++}\exp(-i\,k_{z,\alpha z}^{++}z)).\cos(\theta_\alpha/2) \\ &+ \exp(ik_{//,\alpha}^{+-} r_{//})(a_\alpha^{+-}\exp(i\,k_{z,\alpha}^{+-}z) + b_\alpha^{+-}\exp(-i\,k_{z,\alpha z}^{+-}z)).\cos(\theta_\alpha/2) \\ &+ \exp(ik_{//,\alpha}^{-+} r_{//})(a_\alpha^{-+}\exp(i\,k_{z,\alpha}^{-+}z) + b_\alpha^{-+}\exp(-i\,k_{z,\alpha z}^{-+}z)).e^{-i\varphi_\alpha}\sin(\theta_\alpha/2) \\ &+ \exp(ik_{//,\alpha}^{--} r_{//})(a_\alpha^{--}\exp(i\,k_{z,\alpha}^{--}z) + b_\alpha^{-+}\exp(-i\,k_{z,\alpha z}^{--}z)).e^{-i\varphi_\alpha}\sin(\theta_\alpha/2) \end{aligned}$$

and

$$\begin{aligned} \psi_\alpha^-(r) &= \exp(ik_{//,\alpha}^{++} r_{//})(a_\alpha^{++}\exp(i\,k_{z,\alpha}^{++}z) + b_\alpha^{++}\exp(-i\,k_{z,\alpha z}^{++}z)).e^{i\varphi_\alpha}\sin(\theta_\alpha/2) \\ &+ \exp(ik_{//,\alpha}^{+-} r_{//})(a_\alpha^{+-}\exp(i\,k_{z,\alpha}^{+-}z) + b_\alpha^{+-}\exp(-i\,k_{z,\alpha z}^{+-}z)).e^{i\varphi_\alpha}\sin(\theta_\alpha/2) \\ &+ \exp(ik_{//,\alpha}^{-+} r_{//})(a_\alpha^{-+}\exp(i\,k_{z,\alpha}^{-+}z) + b_\alpha^{-+}\exp(-i\,k_{z,\alpha z}^{-+}z)).\cos(\theta_\alpha/2) \\ &+ \exp(ik_{//,\alpha}^{--} r_{//})(a_\alpha^{--}\exp(i\,k_{z,\alpha}^{--}z) + b_\alpha^{-+}\exp(-i\,k_{z,\alpha z}^{--}z)).\cos(\theta_\alpha/2) \end{aligned}$$

1.4.4 Continuity conditions and matrices.

The eight constants $a_\alpha^\pm$ et $b_\alpha^\pm$ are fixed by the continuity of ψ and $\nabla\psi$ at the interface. This gives exactly 8 equations.

The **M** matrix is then a 8×8 matrix but with 2 non zero 4×4 blocks (there are no cross terms between the group with $k_{//,0}^+$ and the group with $k_{//,0}^-$.

It is possible to split the problem in two calculations using 4×4 matrices.

The continuity relations can be written :

$$\underline{D}_\alpha(\vec r_\alpha)\begin{pmatrix} a_\alpha^{++} \\ b_\alpha^{++} \\ a_\alpha^{-+} \\ b_\alpha^{-+} \\ a_\alpha^{--} \\ b_\alpha^{--} \\ a_\alpha^{+-} \\ b_\alpha^{+-} \end{pmatrix} = \underline{D}_{\alpha+1}(\vec r_\alpha)\begin{pmatrix} a_{\alpha+1}^{++} \\ b_{\alpha+1}^{++} \\ a_{\alpha+1}^{-+} \\ b_{\alpha+1}^{-+} \\ a_{\alpha+1}^{--} \\ b_{\alpha+1}^{--} \\ a_{\alpha+1}^{+-} \\ b_{\alpha+1}^{+-} \end{pmatrix} \tag{1.58}$$

where the 8×8 matrix $\underline{D}_\alpha(\vec r_\alpha)$ is written :

$$\underline{D}_\alpha(\vec r_\alpha) = \begin{pmatrix} \underline{DA}_\alpha & \underline{0} \\ \underline{0} & \underline{DB}_\alpha \end{pmatrix} \tag{1.59}$$

We give here the two matrices written with the notations :

we omit the index α and we write ($\theta' = \frac{\theta_\alpha}{2}$)

$$\underline{DA}_\alpha = \left(\begin{array}{ll} e^{ik_{//}^{++}r}\cos(\theta')e^{ik_z^{++}z} & e^{ik_{//}^{++}r}\cos(\theta')e^{-ik_z^{++}z} \\ k_z^{++}e^{ik_{//}^{++}r}\cos(\theta')e^{ik_z^{++}z} & -k_z^{++}e^{ik_{//}^{++}r}\cos(\theta')e^{-ik_z^{++}z} \\ e^{ik_{//}^{++}r}e^{i\varphi}\sin(\theta')e^{ik_z^{++}z} & e^{ik_{//}^{++}r}e^{i\varphi}\sin(\theta')e^{-ik_z^{++}z} \\ k_z^{++}e^{ik_{//}^{++}r}e^{i\varphi}\sin(\theta')e^{ik_z^{++}z} & -k_z^{++}e^{ik_{//}^{++}r}e^{i\varphi}\sin(\theta')e^{-ik_z^{++}z} \end{array}\right. \tag{1.60}$$

$$\left.\begin{array}{ll} -e^{ik_{//}^{-+}r}e^{-i\varphi}\sin(\theta')e^{ik_z^{-+}z} & -e^{ik_{//}^{-+}r}e^{-i\varphi}\sin(\theta)e^{-ik_z^{-+}z} \\ -k_z^{-+}e^{ik_{//}^{-+}r}e^{-i\varphi}\sin(\theta)e^{ik_z^{-+}z} & k_z^{-+}e^{ik_{//}^{-+}r}e^{-i\varphi}\sin(\theta)e^{-ik_z^{-+}z} \\ e^{ik_{//}^{-+}r}\cos(\theta')e^{ik_z^{-+}z} & e^{ik_{//}^{-+}r}\cos(\theta')e^{-ik_z^{-+}z} \\ -k_z^{-+}e^{ik_{//}^{-+}r}\cos(\theta')e^{ik_z^{-+}z} & k_z^{-+}e^{ik_{//}^{-+}r}\cos(\theta')e^{-ik_z^{-+}z} \end{array}\right)$$

$$\underline{DB}_\alpha = \left(\begin{array}{ll} -e^{ik_{//}^{--}r} e^{-i\varphi} \sin(\theta') e^{ik_z^{--}z} & -e^{ik_{//}^{--}r} e^{-i\varphi} \sin(\theta') e^{-ik_z^{--}z} \\ -k_z^{--} e^{ik_{//}^{--}r} e^{-i\varphi} \sin(\theta') e^{ik_z^{--}z} & k_z^{--} e^{ik_{//}^{--}r} e^{-i\varphi} \sin(\theta') e^{-ik_z^{--}z} \\ e^{ik_{//}^{--}r} \cos(\theta') e^{ik_z^{--}z} & e^{ik_{//}^{--}r} \cos(\theta') e^{-ik_z^{--}z} \\ k_z^{--} e^{ik_{//}^{--}r} \cos(\theta') e^{ik_z^{--}z} & -k_z^{--} e^{ik_{//}^{--}r} \cos(\theta') e^{-ik_z^{--}z} \end{array} \right. \quad ... \tag{1.61}$$

$$... \left. \begin{array}{ll} e^{ik_{//}^{+-}r} \cos(\theta') e^{ik_z^{+-}z} & e^{ik_{//}^{+-}r} \cos(\theta') e^{-ik_z^{+-}z} \\ k_z^{+-} e^{ik_{//}^{+-}r} \cos(\theta') e^{ik_z^{+-}z} & -k_z^{+-} e^{ik_{//}^{+-}r} \cos(\theta') e^{-ik_z^{+-}z} \\ e^{ik_{//}^{+-}r} e^{i\varphi} \sin(\theta') e^{ik_z^{+-}z} & e^{ik_{//}^{+-}r} e^{i\varphi} \sin(\theta') e^{-ik_z^{+-}z} \\ k_z^{+-} e^{ik_{//}^{+-}r} e^{i\varphi} \sin(\theta') e^{ik_z^{+-}z} & -k_z^{+-} e^{ik_{//}^{+-}r} e^{i\varphi} \sin(\theta') e^{-ik_z^{+-}z} \end{array} \right)$$

the matrix $\underline{M}$ is defined by :

$$\underline{M} = \prod_{\alpha=0}^{\alpha=N} \underline{D}_\alpha^{-1}(\vec{r}_\alpha) \underline{D}_{\alpha+1}(\vec{r}_\alpha) = \underline{M} = \begin{pmatrix} \underline{MA} & \underline{0} \\ \underline{0} & \underline{MB} \end{pmatrix} \tag{1.62}$$

where

$$\underline{MA} = \prod_{\alpha=0}^{N} \underline{DA}_\alpha^{-1} \underline{DA}_{\alpha+1} and \quad \underline{MB} = \prod_{\alpha=0}^{N} \underline{DB}_\alpha^{-1} \underline{DB}_{\alpha+1} \tag{1.63}$$

We have the relation :

$$\begin{pmatrix} a_0^{++} \\ b_0^{++} \\ a_0^{-+} \\ b_0^{-+} \\ a_0^{--} \\ b_0^{--} \\ a_0^{+-} \\ b_0^{+-} \end{pmatrix} = \underline{M} \begin{pmatrix} a_s^{++} \\ b_s^{++} \\ a_s^{-+} \\ b_s^{-+} \\ a_s^{--} \\ b_s^{--} \\ a_s^{+-} \\ b_s^{+-} \end{pmatrix} \tag{1.64}$$

In the case of incident "up" neutrons, equation (1.64) gives

$$\begin{pmatrix} 1 \\ r_0^{++} \\ 0 \\ r_0^{-+} \\ 0 \\ 0 \\ 0 \\ 0 \end{pmatrix} = \underline{M} \begin{pmatrix} t_s^{++} \\ 0 \\ t_s^{-+} \\ 0 \\ 0 \\ 0 \\ 0 \\ 0 \end{pmatrix} \tag{1.65}$$

for "down" neutrons we have :

$$\begin{pmatrix} 0 \\ 0 \\ 0 \\ 0 \\ 1 \\ r_0^{--} \\ 0 \\ r_0^{+-} \end{pmatrix} = \underline{M} \begin{pmatrix} 0 \\ 0 \\ 0 \\ 0 \\ t_s^{--} \\ 0 \\ t_s^{+-} \\ 0 \end{pmatrix} \tag{1.66}$$

Let r_0^{++} , r_0^{-+} be the reflectivity amplitudes for a neutron up, reflected up (resp. down), The corresponding transmission coefficients are given by t_s^{++} , t_s^{-+} .

We deduce :

$$\left\{ \begin{array}{l} r_0^{++} = \frac{MA_{21}MA_{33} - MA_{23}MA_{31}}{MA_{11}MA_{33} - MA_{13}MA_{31}} \\ r_0^{-+} = \frac{MA_{41}MA_{33} - MA_{43}MA_{31}}{MA_{11}MA_{33} - MA_{13}MA_{31}} \end{array} \right. and \left\{ \begin{array}{l} t_s^{++} = \frac{MA_{33}}{MA_{11}MA_{33} - MA_{13}MA_{31}} \\ t_s^{-+} = \frac{-MA_{31}}{MA_{11}MA_{33} - MA_{13}MA_{31}} \end{array} \right. \tag{1.67}$$

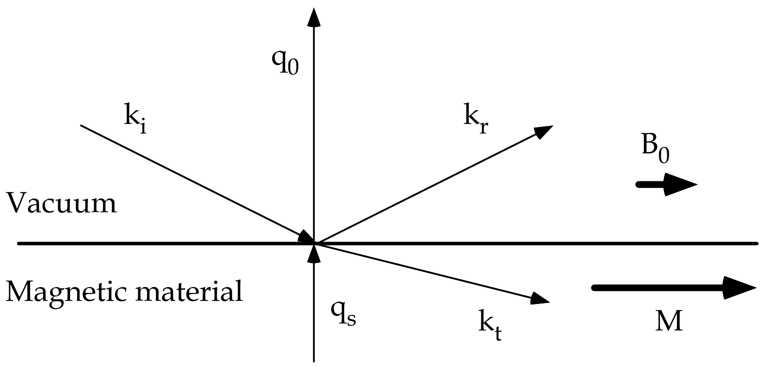

Figure 1.4: incidence of a neutron beam on a magnetic substrate of magnetization **M** in an applied field $\mathbf{B_0}$.

We find similar relations for the 4 other coefficients.
The reflected intensities are given by :

$$I^{++} \propto \left|r^{++}\right|^2 \tag{1.68}$$

and

$$I^{-+} \propto \left|r^{-+}\right|^2 \tag{1.69}$$

In the case of small external magnetic field, we have I $^{+-} \approx$ I $^{-+}$.

1.4.5 Reflection on a magnetic dioptre.

Let q be the (Oz) component of the diffusion vector $\mathbf{q} = \mathbf{k_r} - \mathbf{k_i}$.
We will consider the case of a reflection on a magnetic substrate.
To simplify the problem, we assume that the applied magnetic field $\mathbf{B}_0$ is small so that $q_0^+ \approx q_0^- = q_0$. The component of the $\mathbf{q}$ vector in the magnetic medium is given by (see 1.34) :

$$q_s^{\pm} \approx \sqrt{q_0^2 - 16\pi\rho(b_n \pm b_m)} \tag{1.70}$$

N.B. : we remind that "$q = 2k_z$".
We will assume that the external field $\mathbf{B}_0$ and the magnetization $\mathbf{M}$ lie in the layer plane. This corresponds to $\theta = 90°$ (see figure 1.3). Let ϕ be the angle between $\mathbf{B}_0$ and $\mathbf{M}$.
The expressions of the reflection coefficients deduced from the expressions of the M matrices are given by :

$$r^{++} = \frac{\cos^2\frac{\phi}{2}\ (q_0 - q_s^+)\,(q_0 + q_s^-) + \sin^2\frac{\phi}{2}\ (q_0 - q_s^-)\,(q_0 + q_s^+)}{\cos^2\frac{\phi}{2}\ \left(q_0 + q_s^+\right)\left(q_0 + q_s^-\right) + \sin^2\frac{\phi}{2}\ \left(q_0 + q_s^-\right)\left(q_0 + q_s^+\right)} \tag{1.71}$$

$$r^{+-} = \frac{2\,q_0 \cos\frac{\phi}{2}\ \sin\frac{\phi}{2}\ (q_s^+ - q_s^-)}{\cos^2\frac{\phi}{2}\ \left(q_0 + q_s^+\right)\left(q_0 + q_s^-\right) + \sin^2\frac{\phi}{2}\ \left(q_0 + q_s^-\right)\left(q_0 + q_s^+\right)} \tag{1.72}$$

The measured intensity are given by :

$$I^{++} = \left|r^{++}\right|^2 \quad et \quad I^{+-} = \left|r^{+-}\right|^2 \tag{1.73}$$

Case of a non magnetic substrate.

In this case, corresponding to a zero magnetization ($b_m = 0$), the diffusion vectors q_s^+ and q_s^- are equal (eq. 1.70). The reflection coefficients simplify and can be written in the form of classical Fresnel coefficients :

$$r^{++} = \frac{q_0 - q_s}{q_0 + q_s} \quad et \quad r^{+-} = 0 \tag{1.74}$$

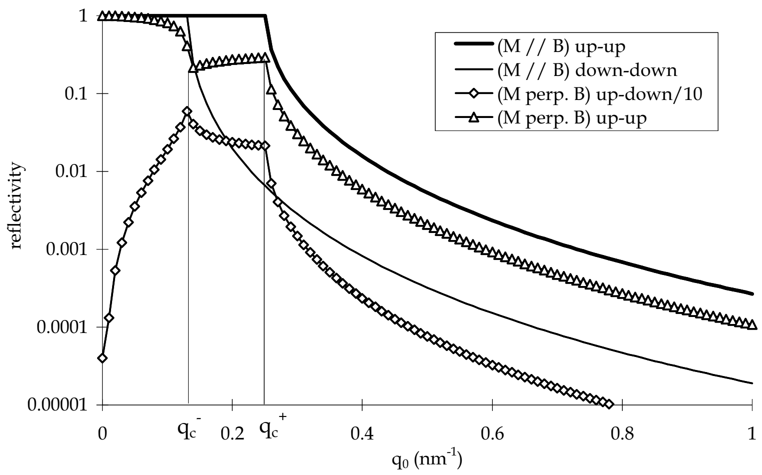

Figure 1.5: reflectivity curves in the case of a magnetization parallel and perpendicular to the magnetic field $\mathbf{B}_0$. When the magnetization is parallel to the field, the non spin flip curves "up-up" and "down-down" are distinct (plain lines), the spin-flip signal is zero. When the magnetization is perpendicular to the field $\mathbf{B}_0$, the spin-flip curves superimpose (squares), a very large spin-flip signal appears (losanges).

The intensity is given by :

$$I^{++} = \left| \frac{q_0 - q_s}{q_0 + q_s} \right|^2 = \left| \frac{q_0 - \sqrt{q_0^2 - q_c^2}}{q_0 + \sqrt{q_0^2 - q_c^2}} \right|^2 \tag{1.75}$$

where the critical wave vector q_c is equal to $\sqrt{16\pi\rho b_n}$. When $q_0 < q_c$, q_s is a pure imaginary number and one finds a reflected intensity equal to 1. When q_0 is very large, one can show that the intensity decreases as $1/q_0^4$.

Case of a magnetic substrate in a magnetic field $\mathbf{B}_0$ aligned with the magnetization M ($\phi = 0$).

In this simple case, the expressions of the reflection coefficients simplify and can be written as :

$$r^{++} = \frac{q_0 - q_s^+}{q_0 + q_s^+}, \quad r^{--} = \frac{q_0 - q_s^-}{q_0 + q_s^-} \quad et \quad r^{+-} = 0 \tag{1.76}$$

These expressions still correspond to Fresnel reflectivities. The only modification introduced by the magnetism is a difference in the critical angle. The critical angles for the reflectivity curves "up-up" and "down-down" are given by :

$$q_c^{\pm} \approx \sqrt{16\pi\rho\,(b_n \pm b_m)} \tag{1.77}$$

The spin-flip signal is zero. N.B. the coefficients r^{++} and r^{--} can be deduced one from the other by a 180° ϕ rotation.

The non spin-flip signals are plotted in plain lines on figure 1.5. We find classical shapes for the reflectivity curves, with a total reflectivity plateau followed by a sharp decrease. The main difference between the "up-up" and "down-down" curves is the extension of the total reflectivity plateau.

Case of a magnetic field perpendicular to the substrate magnetization ($\phi = 90°$).

In this case the reflection coefficients become :

$$r = \frac{(q_0 - q_s^+)\,(q_0 + q_s^-) + \,(q_0 - q_s^-)\,(q_0 + q_s^+)}{2\,\left(q_0 + q_s^+\right)\left(q_0 + q_s^-\right)} = \frac{1}{2}\left(r^{++} + r^{--}\right) \tag{1.78}$$

$$r^{+-} = \frac{q_0\,\left(q_s^+ - q_s^-\right)}{2\left(q_0 + q_s^+\right)\left(q_0 + q_s^-\right)} \tag{1.79}$$

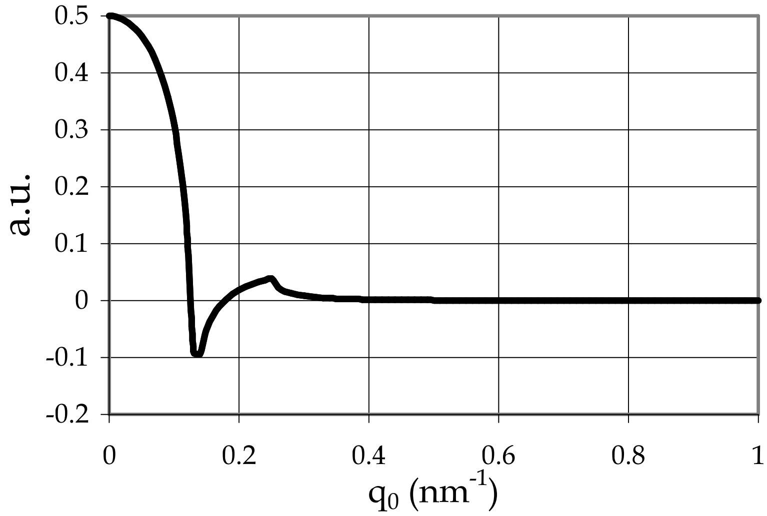

Figure 1.6: contribution of the interference term $Re(r^{++} \times r^{--})$ between the r^{++} and r^{--} amplitudes in the non spin-flip intensities for a reflection on a substrate whose magnetization is perpendicular to the applied magnetic field $\mathbf{B}_0$.

The intensities are given by :

$$I^{++} = I^{--} = |r|^2 = \frac{1}{4}\left|r^{++}\right|^2 + \frac{1}{4}\left|r^{--}\right|^2 + \frac{1}{2}Re\left(r^{++} \times r^{--}\right) \tag{1.80}$$

One can notice that the spin-flip intensities are the sum of three terms. The first two correspond to the intensities of the non spin-flip signals in the case of a magnetization aligned with the external magnetic field ; they are weighted by a $\frac{1}{4}$ coefficient. These terms introduce two discontinuities at the positions q_c^+ et q_c^- in the reflectivity curve (see figure 1.5, white square curve). To these two terms an " interference " term adds $\frac{1}{2}Re\left(r^{++} \times r^{--}\right)$ whose analytical expression is not simple. Its variations are plotted on the figure 1.6. For $q_0 = 0$, this term is equal to $\frac{1}{2}$ and the intensity is totally reflected. Its value decreases as soon as q_0 increases and becomes negative around q_c^- . It becomes positive again around q_c^+ , then decreases very quickly. However, this contribution does not modify qualitatively the form of the non spin-flip curve except that there is no total reflectivity plateau.

The spin-flip intensity is given by :

$$I^{+-} = \left|r^{+-}\right|^2 = \frac{1}{4}\left|\frac{q_0\ \left(q_s^+ - q_s^-\right)}{\left(q_0 + q_s^+\right)\left(q_0 + q_s^-\right)}\right|^2 \tag{1.81}$$

The characteristic form of the spin-flip signal (see figure 1.4) is given by the term $\left|q_s^+ - q_s^-\right|^2$. The variations of this term are plotted on the figure 1.7 (thick lines). Two successive regime changes appear at the points q_c^- and q_c^+ . They correspond to the points where q_s^- and q_s^+ successively changes from pure imaginary to real values.

This signal is slightly modulated by the factor q_0 which gives a linear increase. The factor $1/\left|\left(q_0 + q_s^+\right)\left(q_0 + q_s^-\right)\right|^2$ gives a very fast decrease at large q. Its variations are plotted on figure 1.7 (thin lines).

In the case where the magnetization is not fully perpendicular to the applied magnetic field, the three terms in the I^{++} intensity are weighted by $\cos^4\frac{\phi}{2}$, $\sin^4\frac{\phi}{2}$ and $2\cos^2\frac{\phi}{2}\sin^2\frac{\phi}{2}$ factors, ϕ being the angle between the field and the magnetization.

In the case of a magnetic layer deposited on a non magnetic substrate, the above considerations are not modified. The main difference is that Kiessig fringes appear after the plateau of total reflection.

1.4.6 Inelastic scattering and spin-flip.

When the external field is not zero, there is a difference between the energies of the up and down neutrons. When a spin flip occurs during the reflection, the energy is changed but the parallel components of the

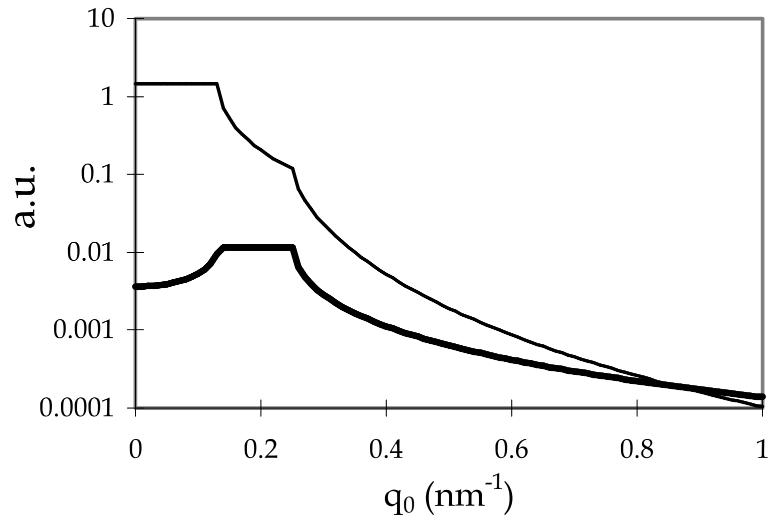

Figure 1.7: variations of two factors of the spin-flip intensity. (bold lines) factor $|q_s^+ - q_s^-|^2$. (thin lines) factor $1/\left|(q_0 + q_s^+)(q_0 + q_s^-)\right|^2$.

wave are conserved. This implies that the spin-flip reflected waves are not exactly aligned with the non spin-flip waves. The difference in angle is easily obtained from the relations (1.57). This has been measured by Felcher and co-workers [30].

1.5 Non perfect layers, practical problems and experimental limits.

1.5.1 Interface roughness

Most of the studied systems show imperfect interfaces depending on the deposition process of the layer. We will consider three roughness scales : interface roughness, interdiffusion and homogeneity of the layer thickness. Let ζ represent the characteristic lateral length-scale for the roughness. A perfect knowledge of the surface would correspond to the knowledge of $z(\zeta)$ for all possible values of ζ. Theoretical approach of the treatment of the roughness are very similar to those described in chapters II and III.

In the field of thin solid films one can distinguish three typical type of roughness which have different origins.

• *Interdiffusion of the species between two successive layers.* This happens during the deposition of a top layer which is miscible with the bottom material. This process is strongly temperature dependent. It corresponds to a typical lengthscale of $\zeta < 0.5\mu m$.

• *A roughness induced by rough edges on the substrate or by grains in the case of two successive layers.* This roughness usually occurs during thin films growth. It is also the type of roughness which is difficult to take into account in models. It corresponds to $1\mu m < \zeta < 100\mu m$.

• *Flatness of the sample.* Depending on the deposition process, the atomic flux may have an angular dependence which can lead to uneven thickness over the sample surface. It corresponds to $\zeta > 100\mu m$.

These three roughness scales can be modeled in three different ways to account for their effects on the measured reflectivity curves. They induce very different effects on the experimental signals.

One has to keep in mind the following limitation : if the lateral fluctuations are not small compared to the layers thicknesses the following treatments are inadequate.

Thickness inhomogeneity of the sample.

The experimental curve simply is the sum of the theoretical curves with different thicknesses. The effect of this type of defects is a blurring of the coherent oscillations for large **q**. Figure 1.8 illustrates this effect.

In a well written simulation program it should be possible to introduce a total thickness fluctuation on top of the global thickness fluctuation of the multilayer. The total thickness fluctuations can be taken into account as an wavelength spread.

Roughness and interdiffusion

Specular reflectivity cannot distinguish between these two type of roughness. The measurement of the coherent scattering length ρb probes a large planar scale compared to the size of the roughness : for a given z depth one measures a mean value of ρb averaged over a large surface.

First solution : Debye-Waller (DW) factor. If one assumes a flat distribution of x, the two types of interface can be treated by a single model where the step function is replaced by the following error function :

$$erf\left(\frac{z-z_\alpha}{\sqrt{2}\sigma_\alpha}\right) = \frac{2}{\sqrt{\pi}}\int_0^{(z-z_\alpha)/\sqrt{2}\sigma_\alpha} e^{-t^2}dt \tag{1.82}$$

This curves shows an inflexion point at z_α. The value σ_α is given by the inverse of the curve slope at z$_\alpha$. The thickness is given by $2\sigma_\alpha$.

The result of 1.82 is to multiply the reflectivity function R of a perfect flat interface by a Debye-Waller factor which can be written [17] :

$$DW = \exp(-2k_\alpha k_{\alpha+1}\sigma_\alpha^2) \tag{1.83}$$

with k_α et $k_{\alpha+1}$ defined by (1.83).

In the case of a stack of multilayers each having a specific roughness, the DW factor is applied to each transfer matrix. Unfortunately, this cannot be applied in the magnetic case, the formalism preventing an easy calculation of the reflectivity R at each interface.

However one can introduce a global DW factor and then apply this DW factor to each diagonal elements at each interface. In practice this works quite well except in the case of rather strong magnetic roughness like domains.

The main effect of this DW factor is to decrease the reflectivity at high **q**.

Second solution : discretisation. This technique is efficient to model interdiffusion.

The interface is replaced by a finite number of discrete layers describing the concentration index. Either an error function or a linear function profile can be used. For real systems of thin solid films, one layer with an average ρb usually works well.

Figure 1.8 shows the effect of roughness on a reflectivity curve measured on a nickel film deposited on a silicon substrate. One can notice on this curve that the discretization induces an intensity decrease at large **q**, as well as a decrease of the interference fringes amplitude.

Intermediate roughness

In the case of the intermediate roughness, the previous methods are not completely satisfactory. Actually, this type of roughness not only decreases the specular reflectivity but also creates a non specular diffuse background which can modify the results. In this case, the diffuse scattering should be measured and the specular reflectivity should be corrected accordingly. This treatment is quite complex and will not be detailed here.

Magnetic roughness.

This problem is very complex. A typical example of magnetic roughness is a demagnetized sample. In this case each domain has an effective diffusion length very different from its neighbor. This appears for neutrons as a giant roughness. There is no simple theoretical way of taking this into account yet. Non specular magnetic measurements can in some cases give the average size of the magnetic domains.

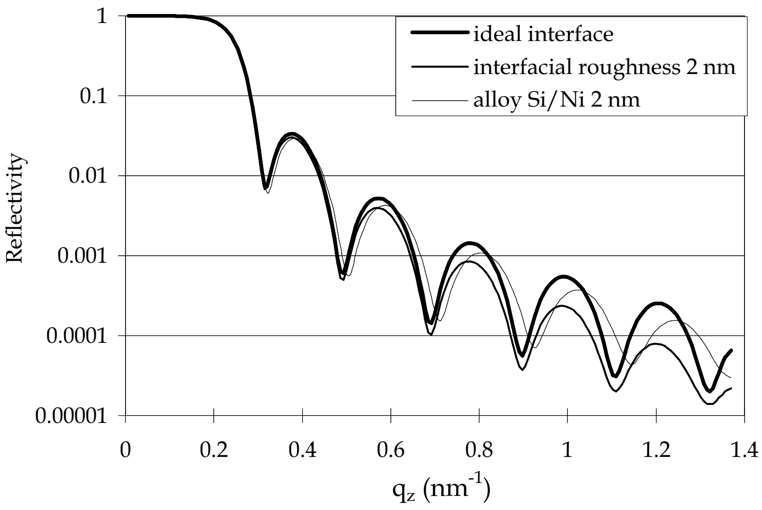

Figure 1.8: roughness effects : comparison between a perfect layer, an 2 nm interfacial roughness, 2 nm Ni-Si interdiffusion at the interface

1.5.2 Angular resolution

The different expressions given above are valid for a perfect incident beam. For the fit of experimental data, it is important to have a good knowledge of the beam divergence and homogeneity.

The beam angular divergence and wavelength dispersion must be taken into account in the simulations.

The divergence of the incident beam , $\delta\theta$, is determined by two slits if the beam is smaller than the effective thickness of the sample or by the first slit and the sample itself at very small angles and when the sample is small.

Usually, $\delta\theta$ is fixed during the experiment. We have then to convolute the calculated reflectivity with a function which is the experimental shape of the beam divergence. However a square function gives in most cases a good approximation of that function.

In the case of curved samples, $\delta\theta$ can be slightly adjusted during the treatment.

$\delta\theta$ has two effects : a decrease of the amplitude of the oscillations and a rounding of the discontinuity at the critical angle. Figure 1.8 gives an example of this effect.

Wavelength dispersion is strongly dependent on the monochromator or on the time resolution in the case of time of flight spectrometers.

The effect of that dispersion is different from an angular divergence : the oscillations disappear at high angles. If a sample has a non homogeneous thickness, the effect is very similar.

1.5.3 Analysis of experimental data

Reflectivity curves cannot be directly inverted. For a non magnetic system, it is even possible to build a family of profiles which give the same reflectivity curve. This is due to the fact that we measure only the intensity and not the phase of the reflectivity [18]. For magnetic systems, the problem of phase is less critical.

However, the main source of uncertainty on the result is in general due to the lack of intensity at high angles.

The analysis of experimental data is done by adjusting the different parameters involved in the problem until a good fit is obtained. In the case of magnetic systems, we usually know rather well the composition of the different layers. We have then to adjust the roughness, the thicknesses and the magnetic moments magnitude.

It is in general very useful to have some external information like X rays reflectometry and magnetic hysteresis curves.

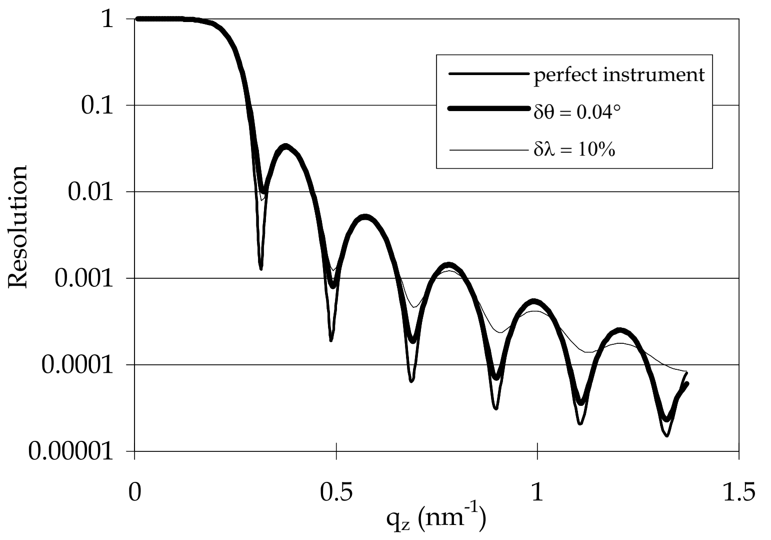

Figure 1.9: Effect of $\delta\theta$ and $\delta\lambda$. Comparison between a perfect instrument, an instrumental $\delta\theta$, and a $\delta\lambda$ for a measurement on a simple one layer system.

1.6 The spectrometers.

1.6.1 Introduction

The spectrometers can be divided in two different groups : time of flight reflectometers like EROS at the Laboratoire Léon Brillouin (LLB), CRISP and SURF at ISIS particularly adapted for liquids and monochromatic reflectometers like PADA at LLB and ADAM at the Institut Laue Langevin (ILL).

1.6.2 Time of flight reflectometers.

The time of flight technique consists in sending a pulsed white beam on the sample. As the speed of the neutron varies as the inverse of the wavelength, the latter is directly related to the time taken by the neutron to travel from the pulsed source to the detector (L) by :

$$\lambda = \frac{h}{mL}t \tag{1.84}$$

That relation is also written as :

$$\lambda(nm) = \frac{t(\mu s)}{2527L(m)} \tag{1.85}$$

On a spallation source, the neutron beam is pulsed and the time of flight technique is used. On a reactor, pulsed neutrons are produced by a chopper.

For a reflectivity measurement, the angle is fixed and the curve is obtained by the separation for the different wavelengths. Sometimes, it is necessary to use several angles because the domain of diffusion vector q_z is not large enough.An example of time of flight spectrometer is presented on figure 1.10.

1.6.3 Monochromatic reflectometers

Monochromatic reflectometers are basically two axes spectrometers. The wavelength is fixed (0.4 nm for PADA) and the reflectivity curve is obtained by changing the incident angle θ. In this case, the sample is usually vertical.

On this type of reflectometers it is easy to put a polarizer and an analyzer in order to select the spin states of the incident and reflected neutrons.

The flippers can be of Mezei type (2 orthogonal coils) [20] and allow to flip the neutron spin state from up to down. The polarizing mirrors are fabricated at the Paul Scherrer Institut [25]. An example of two-axis spectrometer is presented on figure 1.11.

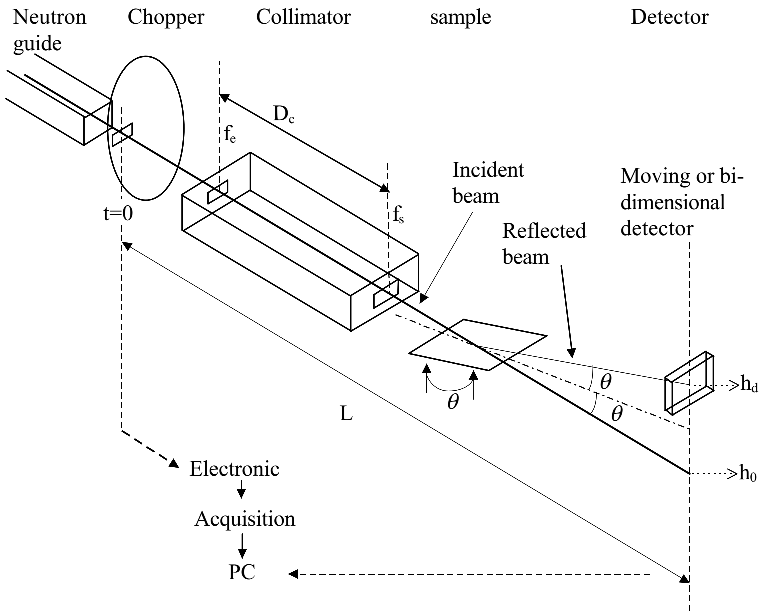

Figure 1.10: Description of the time of flight reflectometer EROS at the LLB [19].

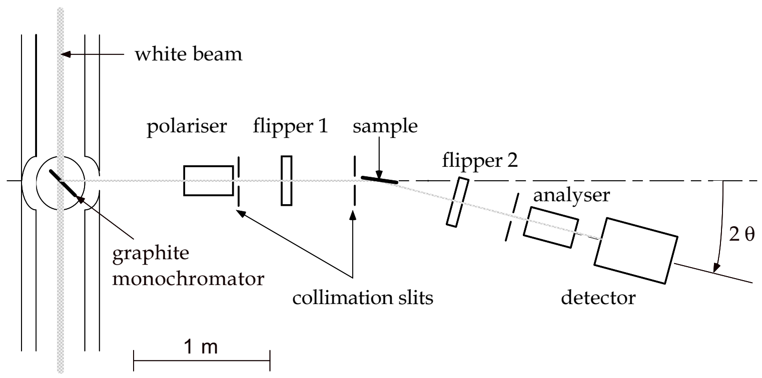

Figure 1.11: the two axis reflectometer PADA at the LLB.

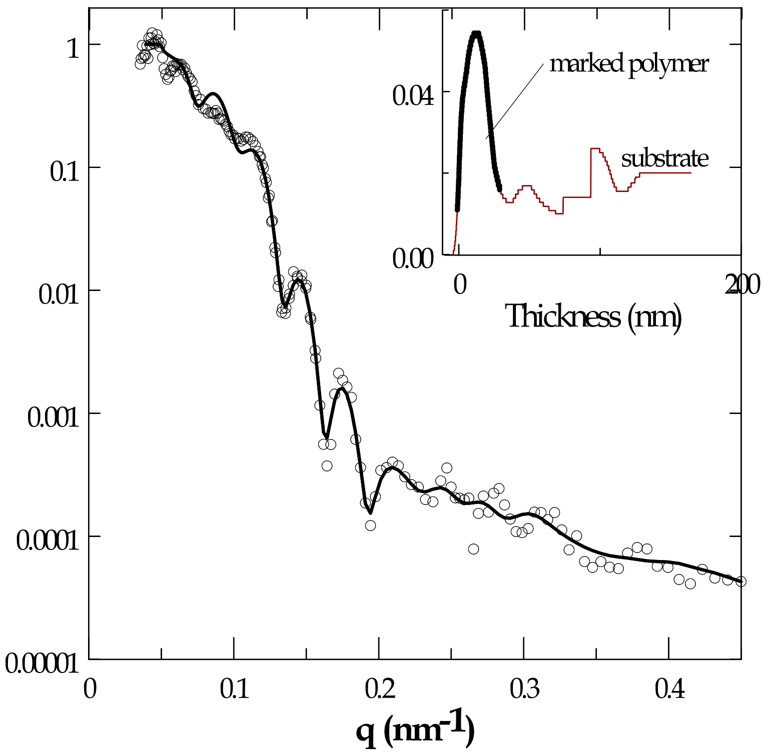

Figure 1.12: Reflectivity of a bilayer, polystyrene on deuterated polystyrene.

1.7 Polymer examples.

Reflectometry is largely used for soft matter due to the large penetration of the neutron beam and the large contrast between deuterated and protonated systems. We give here two examples done on the reflectometer EROS.

1.7.1 Interdiffusion between two layers.

Reflectivity is usually well adapted for polymers because the probed distances are of the same order as the polymer lengths. Moreover, due to the large difference of scattering lengths between hydrogen ($b = -3.7fm$) and the deutérium ($b = 6.67fm$), it is possible to obtain an excellent contrast for the reflectivity measurements by selective deuteration [21, 22].

By spin coating, it is possible to deposit polymers on glass or silicon with a roughness below 1 nm. It is then possible to deposit a second layer on the first one. If one of the layer is deuterated, it is possible to study the interdiffusion as a function of time and temperature annealing. That diffusion will appear as a smearing of the interface and so a decrease of the Kiessig fringes amplitude (see figure 1.13).

1.7.2 Interdiffusion between several layers

Diblock copolymers are made with two chains A and B attached together. These systems present a large variety of interesting properties. For example, if A and B are not miscible, they can form layers with a fixed thickness parallel to the surface where the solution is deposited. The use of a deuterated part A allow us to study the diffusion of the molecules perpendicularly to the surface. Such results are presented in the next figure.

The initial system corresponds to layer of copolymer partially deuterated deposited on a trilayer of totally hydrogenated polymer.

The system has been annealed for 12 hours at 400 K and then remeasured (right curve). We then see a clear Bragg peak which implies a diffusion of the polymers to the inner layers.

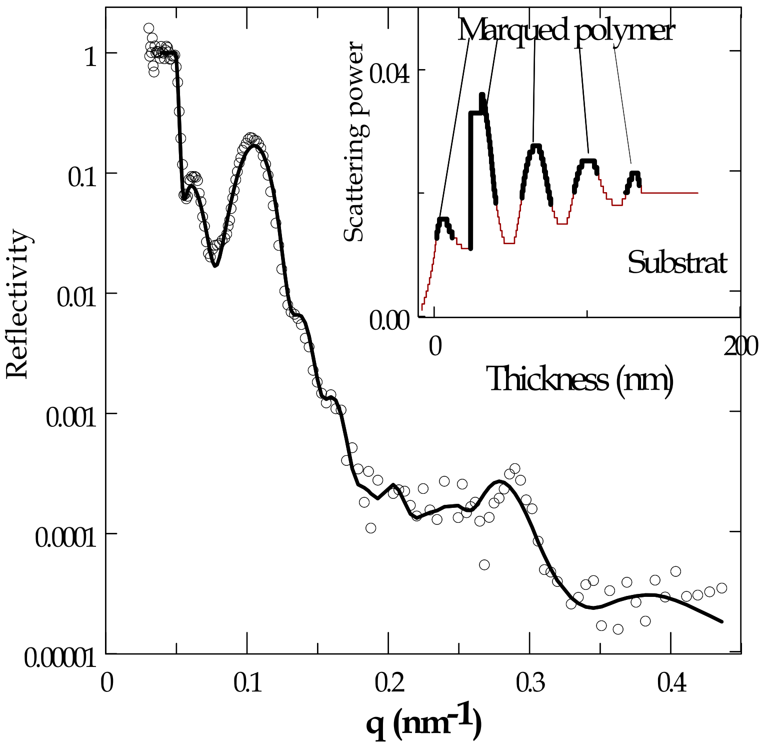

Figure 1.13: Reflectivity of a bilayer, polystyrene on deuterated polystyrene after annealing for 1 hour at 115C.

1.8 Examples on magnetic systems.

In this part, we shall give some examples in order to highlight the different information that can be obtained by polarized neutron reflectometry. All the experiments shown here have been done on the reflectometer PADA.

1.8.1 Absolute measurement of a magnetic moment.

Neutron reflectometry can be used to measure absolute moments (in μ_B per atom). The obtained value is independent of the layer thickness and of the surface of the sample.

As an example, figure 13 shows a curve obtained on a NiFe single layer. By fitting the curves, we obtain the ratio between Ni and Fe with an error of about 2% and the absolute moment with a precision of about $0.02\mu_B$. That measurement took only 15 minutes on a 1 cm^2 sample.

1.8.2 Bragg peaks of multilayers.

Periodic multilayers

In the case of periodic multilayers, we can observe Bragg peaks corresponding to the period of the multilayer. In the case of antiferromagnetic coupling or variable angle coupling, it is possible to obtain directly a mean angle between the different magnetic layers. With polarized neutrons, it is possible to measure very rapidly a precise value of the average moments. If high order Bragg peaks are observed, a good estimate of the chemical and magnetic interface can be obtained. In the literature, there is a large amount of results on multilayers [18, 23, 24].

Supermirrors [25]

If a non periodic multilayer with an almost continuous variation of the period is built, this correspond to add a large number of Bragg peaks just behind the total reflectivity plateau. By that that technique it

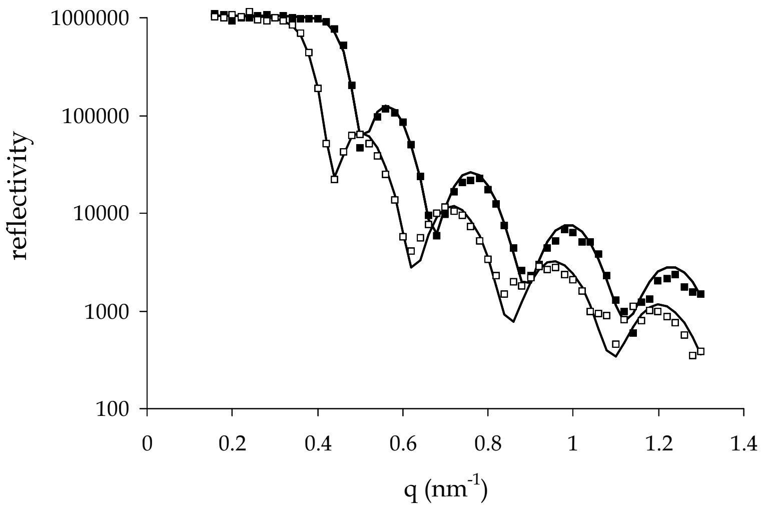

Figure 1.14: reflectivity curve on a 25 nm thick NiFe layer. Black squares are the R^{++} and white squares R^{--}.

is possible to enhance the width of this plateau by a factor 3 or 4. Such mirrors are now widely used for neutron guides and for polarization devices. Figure 1.15 gives an example of a polarizing mirror.

1.8.3 Measurement of the in-plane and out of plane rotation of moments. Measurement of the moment variation in a single layer.

This kind of measurement is perhaps the most important information given by polarized neutron reflectivity (PNR) for magnetic thin films.

We shall give here 2 examples of determination of in-depth magnetic profiles.

Out of plane rotation of the moments in Au/Co/Au. (collaboration with IEF, Orsay France)[26]

In the case of very thin cobalt layers, thinner than 2.5 nm, the magnetization is perpendicular to the surface layer.

We have studied a 3 nm thick Co layer sandwiched between two Au layers. Magneto-optic Kerr effect measurements have shown that the moment is mainly in-plane but with a small out of plane contribution. In order to understand the magnetic behaviour of such a layer, we have fitted the PNR curves with two different models : for the first one, we have considered that the whole layer was uniformly aligned. In the second one, we have allowed a rotation in the layer. The figure 1.16 gives the reflectivity curves and the figure 1.17 gives the corresponding model.

Rotation in strained Nickel layers.

In single magnetic thin films, the microstructure can be such that the magnetoelastic (ME) properties vary throughout the sample thickness : a gradient of the ME coefficient $B(z)$ can appear, related to surface relaxation effects. It can be written in a form similar to surface anisotropy constants [27].

$$B(z) = B_{bulk} + \frac{B_{surf}}{(z - z_0)} \tag{1.86}$$

where z is the depth in the thin film and z_0 an adjustable parameter.

When a mechanical strain is applied on a magnetic thin film, the magnetization tends to rotate either along or perpendicular to the applied strain. A ME coefficient gradient will then lead to a gradient of magnetization rotation though the thin film. This has been measured on single nickel layers as illustrated on figure 1.18. The numerical fit shows that the average rotation under a 0.03% deformation is 30° but there is a 15° gradient of rotation between the surfaces and the bulk of the material [28].

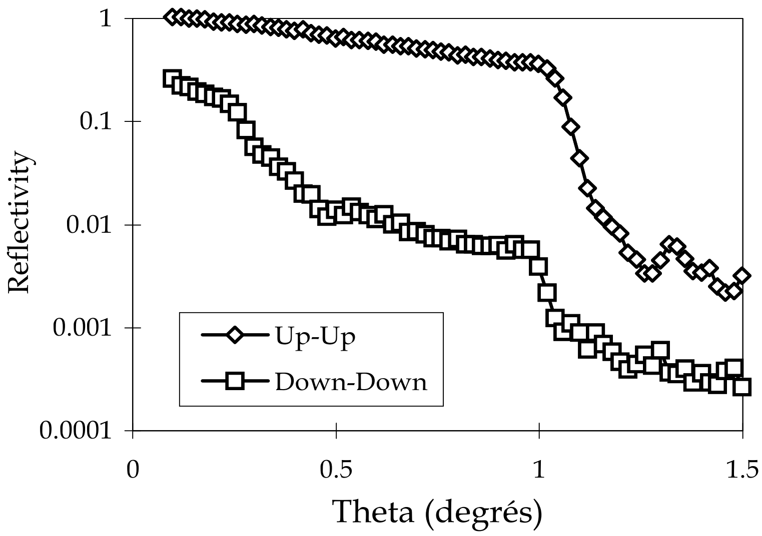

Figure 1.15: Example of a polarizing mirror. The two curves correspond to each state of incident neutron spin.The small dip seen at $0.06 \mathring{A}^{-1}$ is due to the absence of a Bragg peak at that particular position.

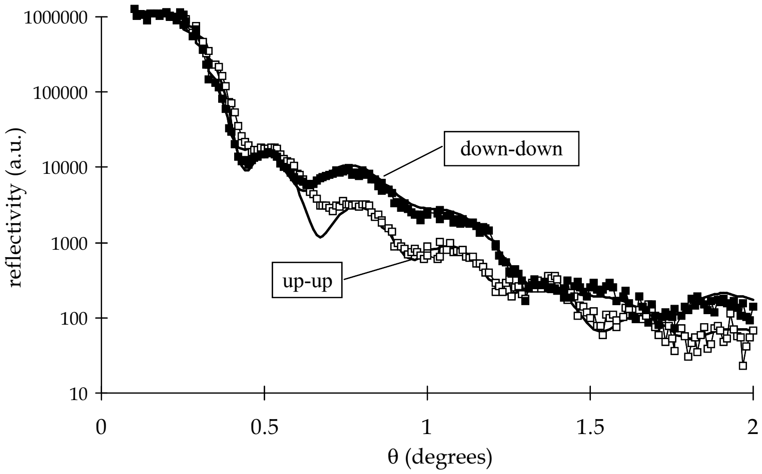

Figure 1.16: reflectivity curve of a Au/Co(3nm)/Au trilayer system.

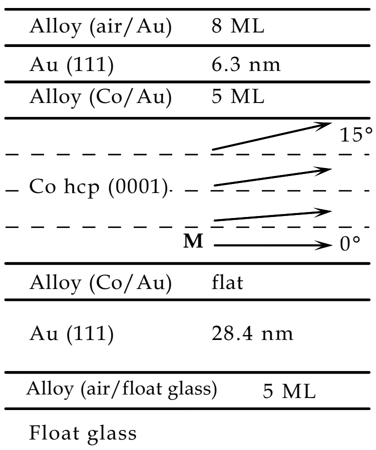

Figure 1.17: thicknesses and moment directions giving the best fit of the reflectivity curves.

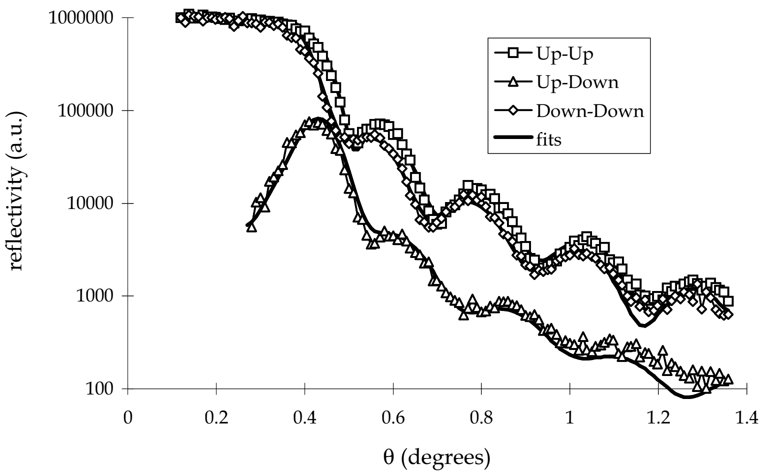

Figure 1.18: Reflectivity curves on a strained nickel layer (thickness 40 nm) for each state of neutron spin. The deformation applied to the substrate is 0.03 %.

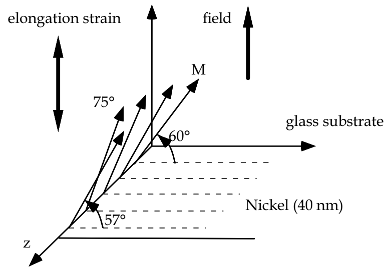

Figure 1.19: Diagram showing the magnetization rotation gradient deduced from the neutron fit.

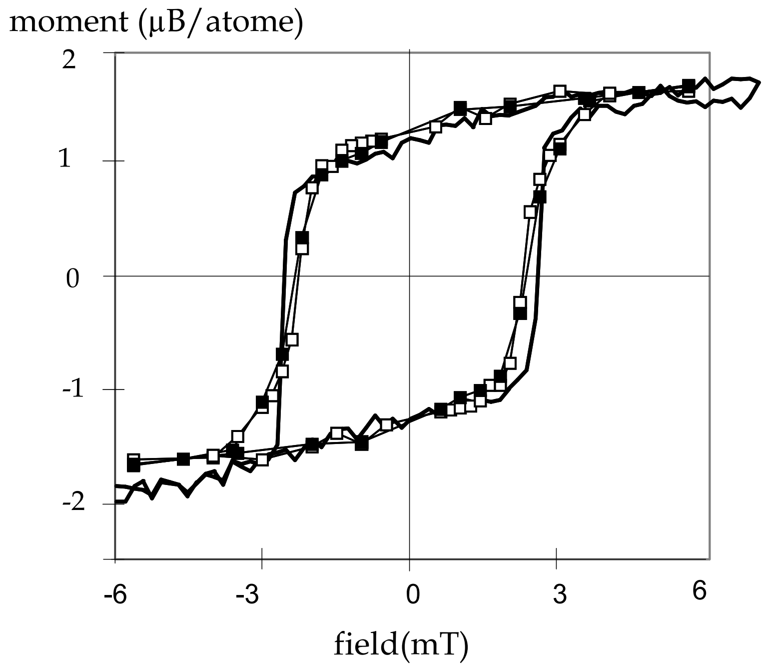

Figure 1.20: Hysteresis loops measured for a single cobalt layer : by MOKE (continuous curve) and from the reflectivity measurements at only one angle (0.3 deg white squares, 0.4 deg black squares).

1.8.4 Selective hysteresis loops.[29]

A complete set of reflectivity curves (R^{++}, R^{--} and R^{+-}) takes about 12 hours to be performed. If we want to follow the magnetization of different layers as a function of field or temperature, the total experiment would be far too long compared to the time usually allocated on a neutron reflectometer (typically one week per year). So the idea is the following : from the fits of the reflectivity curves in the saturated state we know the different thicknesses and magnetic states of the multilayer system. We are then able to calculate the reflectivity curves for different module and orientation of the magnetic layers. It is then not necessary to perform complete reflectivity curves for each value of field but we can measure only the reflectivity for $(n+1)q$ values well chosen where n is the number of different magnetic layers. Comparison of the experimental values obtained and calculation using the parameters obtained from the saturated state allows us to rebuild the magnetic evolution as a function of the applied external field.

Figure 1.20 give the example of an hysteresis loop obtained for a single magnetic layer. Figure 1.21 corresponds to a more complicated system : substrate /Pt(98Å) /Co(7.6Å) /Pt(33Å) /Co(3.8Å) /Pt(32Å). Such a technique has given the moment of each layer separately.

The sum of the two magnetizations agrees well with the magnetization given by conventional measurements and the saturation value of each layer corresponds to the values measured on other samples with just one layer.

1.9 Conclusion on neutron reflectometry

This chapter has given an overview of the neutron reflectometry as a tool for the investigation of surfaces. We have presented a matrix formalism which makes it possible to describe the specular reflectivity on non magnetic and magnetic systems. Neutron reflectivity is especially suited for polymer and magnetic thin film systems. This has been illustrated with a few typical examples.

We have not given here examples of non-specular and surface diffraction experiments. This kind of experiment has suffered until now from the lack of intensity on the neutron spectrometers and from the fact that the formalism necessary to analyze the experiments is still being developed.

The neutron has a good energy for inelastic scattering on condensed matter but we have not spoken here on this aspect of reflectometry which is rather new. A beautiful example of inelastic scattering is

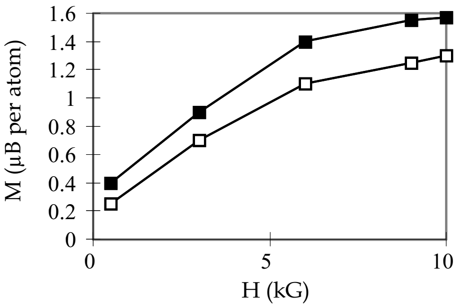

Figure 1.21: magnetization of each magnetic layer of a /Pt(98Å) /Co(7.6Å) /Pt(33Å) /Co(3.8Å) /Pt(32Å) thin film. The white squares correspond to the thinnest layer.

the measurement of the Zeeman energy (see 1.57 and [30]).

The problem of phase determination in neutron reflectometry is also an active field of research [31, 32, 33]. If not only the intensity but also the phase of the reflectivity can be measured a direct inversion of the reflectivity profile would be possible.

Bibliography

[1] G.P. Felcher, R.O. Hilleke, R.K. Crawford, J. Haumann, R. Kleb and G. Ostrowski, Rev. Sci. Instr **58**, pp. 609 (1987).

[2] C. F. Majkrzak, J. W. Cable, J. Kwo, M. Hong, D. B. McWhan, Y. Yafet and J. Waszcak, Phys. Rev. Lett. **56,** pp. 2700 (1986).

[3] J. Penfold, R.K. Thomas, J. Phys. Condens. Matter **2**, pp. 1369-1412 (1990).

[4] T.P. Russel, Mat. Sci. Rep. **5**, pp.171-271 (1990); T.P. Russel, Physica B **221**, pp.267-283 (1996).

[5] L.T. Lee, D. Langevin, B. Farnoux, Phys. Rev. Lett. **67**, 2678-81 (1991)

[6] J. Penfold, E.M. Lee, R.K. Thomas, Molecular Physics **68**, 33-47 (1989)

[7] M.N. Baibich et al, Phys. Rev. Lett. **61**, 2472 (1988)

[8] V.F. Sears, Physics Report **141**, pp. 281 (1986)

[9] X.L. Zhou, S.H. Chen, Physics Reports **257**, pp. 223-348 (1995).

[10] H. Glättli and M. Goldman, *Methods of experimental Physics, Vol 23, Neutron Scattering* (Academic Press, Orlando, 1987).

[11] S. Dietrich, A. Haase, Physics Reports **260**, 1-138 (1995).

[12] V.F. Sears, *Methods of Experimental Physics*, vol 23A, Neutron Scattering (Academic Press, Orlando, 1987); V.F. Sears, Neutron News **3**,(1992).

[13] J. Lekner, *Theory of reflection of electromagnetic and particle waves* (Martinus Nijhoff, Dordrecht, 1987).

[14] S.J. Blundell and J.A.C. Bland, Phys. Rev. B **46**, pp. 3391 (1992).

[15] C. Fermon, C. Miramond, F. Ott, G. Saux, J. of Neutron Research **4**, pp. 251 (1996).

[16] Pleshanov Z., Physica B **94**, pp. 233-243 (1994).

[17] L. Nevot and P. Croce, Revue de Physique Applique **15**, 761 (1980).

[18] C.F. Majkrzak, Physica B **221**, pp. 342-356 (1996).

[19] B. Farnoux, Neutron Scattering in the '90, Conf. Proc. IAEA in Jülich, 14-18 janvier 1985, pp.205-209, Vienne, 1985, X.D.

[20] F. Mezei, Z. Phys. **255**, pp. 146 (1972).

[21] T.P. Russel et al, Macromolecules **24**, 5721-5726 (1991).

[22] X. Zhao et al, Phys. Rev. Lett. **69**, 776 (1992).

[23] YY. Huang, G.P. Felcher and S.S.P. Parkin, J.M.M.M. **99**, pp. 31-38 (1991).

[24] A. Schreyer, J.F. Aukner, T. Zeidler, H. Zabel, C.F. Majkrzak, M. Schaefer and P. Gruenberg, Euro. Phys. Lett., pp. 595-600 (1995).

[25] P. Boni, Physica B **234-236**, 1038-1043 (1997).

[26] E. Train, C. Fermon, C. Chappert, A. Megy, P. Veillet and P. Beauvillain, J.M.M.M. **156**, pp. 86 (1996).

[27] O. Song, C.A. Ballentine, R.C. O'Handley, Appl. Phys. Lett. **64**, pp. 2593 (1994).

[28] F. Ott, C. Fermon , Physica B **234-236**, pp. 522 (1997).

[29] C Fermon, S. Gray, G. Legoff, V. Mathet, S. Mathieu, F. Ott, M. Viret and P. Warin, Physica B **241-243**, pp. 1055 (1998).

[30] G.P. Felcher, S. Adenwalla, V.O. De Haan and A.A. Van Well, Nature **377**, pp. 409 (1995); G.P. Felcher et al, Physica B **221**, 494-499 (1996).

[31] C.F. Majkrzak and N.F. Berk, Phys. Rev. B **52**, pp. 10827 (1995).

[32] C.F. Majkrzak and N.F. Berk, Phys. Rev. B **58**, pp. 15416 (1998).

[33] J. Kasper et al, Phys. Rev. Lett. **80**, 2614-2617 (1998).

[34] J. Penfold, R.C. Ward, W.G. Williams, J. Phys. E. : Sci. Instrum. **20**, pp. 1411 (1987)

[35] R. Pynn, Phys.Rev. B **45,** pp. 602 (1992).

[36] S.K.Sinha, E.B. Sirota, S. Garoff and H.B. Stanley, Phys.Rev. B **38,** pp. 2297 (1988).

[37] Sun, Thèse de l'Université Paris Sud, Orsay, (1988).

[38] J. Tappert, C. Fermon and R.A. Brand, Physica B **213-214**, pp. 239-241 (1995).